

# *Caenorhabditis elegans* Perilipin Is Implicated in Cold-Induced Lipolysis and Inhibits Autophagy in Early Embryos

(Perilipin / lipolysis / hormone-sensitive lipase / autophagy / lipophagy / *Caenorhabditis elegans*)

F. KAŠŠÁK, A. A. CHUGHTAI, S. KAŠŠÁK, M. KOSTROUCHOVÁ

Biocev, First Faculty of Medicine, Charles University, Vestec, Czech Republic

**Abstract.** Animals use neutral lipids, particularly triacylglycerols (TAGs), to store energy. TAGs are universally organized into dynamic cytoplasmic structures called lipid droplets (LDs). In mammals TAG breakdown is catalysed by lipases, such as hormone-sensitive lipase (HSL). LD membrane-resident proteins called perilipins (PLINs) regulate some of these lipases. The model organism *Caenorhabditis elegans* has a single known PLIN homologue and orthologues of most lipases including HSL. HOSL-1 (the HSL orthologue in *C. elegans*) is responsible for production of cryoprotective glycerol in cold conditions, in addition to its role in fasting-induced lipolysis. We employed this model of cold exposure to study the role of PLIN-1 in the regulation of HOSL-1. Our results suggest that both HOSL-1 and PLIN-1 are required for cold tolerance and for lipid breakdown in cold. However, the loss of PLIN-1 partially rescued the phenotype of *hosl-1* null mutants exposed to cold, suggesting the presence of an alternative pathway generating glycerol via lipolysis. In early embryos, PLIN-1 knock-out results in accumulation of lipids and formation of cytoplasmic clusters of autophagic marker LGG-1, supporting the role of autophagy as an alternative lipolytic pathway in *C. elegans*, as is the case in mammals.

## Introduction

Most eukaryotic organisms use neutral lipids, most importantly triacylglycerols (TAGs), for storage of excess energy. These predominantly reside in lipid droplets (LDs), dynamic cytoplasmic structures with a core of neutral lipids surrounded by a single layer of phospholipids and a coat of LD-associated proteins. In fasting, neutral lipids are catabolized in a tightly regulated and evolutionarily conserved way. Two distinct pathways mediate the degradation of neutral lipids in mammals: cytoplasmic lipolysis and lipolytic autophagy called lipophagy (Sztalryd and Brasaemle, 2017).

The cytoplasmic lipolysis consists of gradual hydrolysis of TAG to diacylglycerol (DAG), monoacylglycerol (MAG) and ultimately to free glycerol, always removing one non-esterified fatty acid (NEFA). Cytoplasmic lipases mediate this catabolism, of which the most important in mammals and in *Caenorhabditis elegans* alike are: adipocyte triglyceride lipase (ATGL) and hormone-sensitive lipase (HSL), with their respective nematode orthologues ATGL-1 and HOSL-1. While ATGL catalyses the first rate-limiting step of TAG to DAG hydrolysis, HSL can catalyse all three steps, but with lower reaction rate. Both of these lipases are regulated by extrinsic signalling, mainly by protein kinase A (PKA), via perilipins (Sztalryd and Brasaemle, 2017).

Perilipins (PLINs) are a group of LD-associated proteins that show a remarkable degree of evolutionary conservation. In human, five distinct PLIN paralogues have been identified to date, all with differential tissue expression profiles and distinct functions. PLIN-1 is the dominant lipolysis regulator in white adipose tissue (Sztalryd and Brasaemle, 2017). Previously, the *C. elegans* locus W01A8.1 (originally annotated as *mdt-28*) was identified as the sole currently known *PLIN* gene orthologue in this nematode, henceforth annotated *plin-1* (Chughtai et al., 2015). This protein was also identified as one of the most abundant LD proteins influencing lipid metabolism (Na et al., 2015; Vrablik et al., 2015).

In mammals, PLINs regulate the cytoplasmic lipolysis both positively and negatively in response to PKA signalling. PKA-polyphosphorylated PLIN-1 activates lipolysis by recruiting HSL to LDs (Sztalryd et al.,

---

Received November 25, 2020. Accepted December 30, 2020.

This work was supported by the European Regional Development Fund (CZ.1.05/1.1.00/02.0109), the LQ1604 National Sustainability Programme II (Project BIOCEV-FAR) and project Biocev (CZ.1.05/1.1.00/02.0109) from the MEYS CR; and by the grants Progress Q26/LF11, SVV 260517/2020, SVV 260377/2017, and SVV 260257/2016 from Charles University.

Corresponding author: Filip Kaššák, Biocev, Průmyslová 595, 252 50 Vestec, Czech Republic. E-mail: filip.kassak@me.com

Abbreviations: ATGL – adipocyte triglyceride lipase, CARS – coherent anti-Stokes Raman scattering, DAG – diacylglycerol, HSL – hormone-sensitive lipase, LDs – lipid droplets, MAG – monoacylglycerol, NEFA – non-esterified fatty acid, PKA – protein kinase A, PLIN – perilipin, TAG – triacylglycerol.

2003) and by releasing CGI-58, co-activator of ATGL (Subramanian et al., 2004). Contrarily, de-phosphorylated PLINs hinder the access of HSL to LD lipids and prevent CGI-58 from binding ATGL on the surface of LDs (Sztalryd et al., 2003; Subramanian et al., 2004). An alternative lipolytic pathway also exists in mammals. In lipophagy, a type of selective autophagy, acidic lipases catabolize neutral lipids in lysosomes (Cingolani and Czaja, 2016). Lipophagy was first described in mouse hepatocytes (Singh et al., 2009) and has since been found to procure neutral lipid breakdown in a variety of organisms and tissues (Sztalryd and Brasaemle, 2017).

Previous work in *C. elegans* found that the absence of PLIN-1 interferes with lipid metabolism, but lipolysis still occurs (Chughtai et al., 2015; Na et al., 2015; Vrablik et al., 2015). The most striking phenotype described in PLIN-1-deficient animals was accumulation of distorted LDs around the nuclei of early-stage embryos. Somatic tissues had contrarily smaller LDs with less lipid content. It was suggested that this could be explained by the presence of a secondary lipolytic pathway that does not depend on PLIN-1-mediated activation (Chughtai et al., 2015).

In *C. elegans*, HOSL-1 is also important for protection against cold. When *C. elegans* is exposed to temperatures close to 0 °C, accumulation of cAMP in cells triggers activation of PKA. Then, PKA activates HOSL-1 by an unknown mechanism. Finally, HOSL-1 catabolizes TAGs while liberating glycerol, which acts as a cryoprotective substance (Liu et al., 2017). However, the role of PLIN-1 in this pathway is not known.

In the currently presented work, we venture to establish whether PLIN-1 could mediate the PKA-dependent activation of HOSL-1 in *C. elegans* exposed to cold. We employ genetically modified knock-out lines to demonstrate that both HOSL-1 and PLIN-1 are needed for efficient cold survival. Moreover, we study the autophagic activity in early embryos of PLIN-1 mutants to illustrate the possible role of autophagy in the lipid metabolism of *C. elegans*.

## Material and Methods

### Transgenic lines

The VS20 [*atgl-1p::atgl-1::GFP + mec-7::RFP*] line was obtained from the Caenorhabditis Genetic Center of the University of Minnesota (Minneapolis, MN) and the tm2369 [*hosl-1<sup>-/-</sup>*] line from the National BioResource

Project (Tokyo, Japan). The RD204 [*P<sub>pie-1</sub>-lgg-1::gfp*] line was a gift from Dr Legouis (Manil-Ségalen et al., 2014). The strain KV1 [*plin-1(KV1)*] was prepared previously by Cas9/CRISPR-induced gene deletion (Chughtai et al., 2015). VS20, tm2369 and RD204 were crossed with KV1 to produce KV7, KV10 and KV2, respectively. Successful progeny of the crossed worms was screened by single-worm PCR as described previously (Chughtai et al., 2015) or by fluorescent microscopy, and the final line was sequenced at target loci to confirm the genotype. Primers used in single-worm PCR-based screening are listed in Table 1.

### Cold resistance experiment

Synchronized L1 larvae of the VS20, tm2369, KV7 and KV10 lines were prepared as described (Stiernagle, 2006) and 20–50 animals per line were seeded onto NGM plates with the OP50 *Escherichia coli* strain and grown to young adults. At this point, the plates were placed in an incubator with a stable temperature between 0 and 0.5 °C and left without interference for 40 h. Thereafter, the plates were left for one hour at 22 °C and then scored. Animals with no pharyngeal pumping and no responsiveness to touch were scored as dead, all others as alive. The experiment was repeated three times and the survival percentage was summed. A z-test for the proportion of two populations in R (R Core Team, 2014) was used to determine statistical significance. Animals scored as alive were stained with the LipidTox (Red) fluorescent dye (Invitrogen, Waltham, MN) as described previously (O'Rourke et al., 2009) with modifications as in Chughtai et al. (2015).

### Microscopy and image analysis

Fluorescent microscopy of LipidTox-stained animals and Nomarski optics bright-field microscopy were done using an Olympus BX60 microscope equipped with a DP30BW CD camera (Olympus, Tokyo, Japan). Confocal images of GFP-expressing animals and coherent anti-Stokes Raman scattering (CARS) images were acquired using a Carl Zeiss LSM 880 NLO microscope (Carl Zeiss AG, Oberkochen, Germany) with the Chameleon Ultra II and Chameleon Compact OPO MP lasers (Coherent, Santa Clara, CA) and an LD C-Apochromat 40x/1.1 W Corr M27 objective (Carl Zeiss), operated by ZEN 2.1 Black program. In CARS microscopy, the sample was concurrently excited by a Pump beam at 807 nm and a Stokes beam at 1050 nm, and an MBS 760++ beam splitter was used to filter out infra-

Table 1. Primers used in single-worm PCR to screen lines

Purpose	Sequence
plin-1 swPCR	5'-CGTACAAACGGTATTTTTATATCGCTTTCCAAAATCTTCGTTTC-3'
	5'-TAACCTAGGTCGAGGGATTTGGACTTTAAGAATGG-3'
hosl-1 swPCR	5'-CTATCGGGGCTCTTCATTTATTCCA-3'
	5'-GGTGGATCTCAATCAATAGTGTCTCTTG-3'

red signal. Scattering was detected at 655 nm, corresponding to the C-H bond energy of  $2870\text{ cm}^{-1}$ . Acquired 8-bit and 16-bit images were edited and analysed using ImageJ in the Fiji distribution (Schindelin et al., 2012).

Morphometric analysis was performed on red channel fluorescent images of LipidTox-stained surviving animals. LipidTox-positive structures were differentiated using a threshold function setting with the cut-off values of 40–255 and 70–255 determined by the lowest possible intensity permitting maximization of the number of individualized structures while subtracting background noise. The “analyse particles” function was applied to an area of anterior gut between pharynx and vulva to determine the absolute and relative area of LipidTox-positive structures. The ANOVA statistical test in R (R Core Team, 2014) was performed to determine statistical significance.

Simultaneous fluorescent confocal and CARS images of RD204 and KV2 young adults were captured as spectral hyperstacks with  $30.8\ \mu\text{m}$  z-dimension covering the thickness of the worm middle body, alongside their corresponding bright-field images. GFP emission channel and CARS channel were extracted and a  $15.4\ \mu\text{m}$  z-stack, covering as much as possible of the earliest embryos, was selected. First embryos were cropped and analysed using the 3D Object Counter tool with the background suppression intensity threshold of 40–255 and a minimal size filter of 5 px. Sums of particle volumes, surfaces and integrated intensity alongside the number of particles per embryo were averaged from at least ten biological replicates. Two-sided unpaired *t*-test in R (R Core Team, 2014) was used to determine statistical significance.

## Results

### *Cold exposure tolerance is decreased in the absence of either HOSL-1 or PLIN-1*

The *plin-1(KV1)* mutant was crossed with a *hosl-1(tm2369)* null mutant. A control line, both single mutants and the resulting *plin-1 hosl-1* double mutant were exposed to temperatures of  $0\text{--}0.5\ ^\circ\text{C}$  for 40 h. Animals lacking the functional *hosl-1* gene had significantly lower survival than controls. The cold tolerance of *plin-1* mutants was lower than that of controls, but higher than that of *hosl-1* mutants. Surprisingly, *plin-1 hosl-1* double mutants had better survival than *hosl-1* mutants, and almost equivalent survival to that of *plin-1* mutants (Fig. 1A).

In controls, cold induced a physiological response of embryo retention, but less severe anatomical defects with often completely preserved gut and gonad structure (Fig. 1B–E). There was less embryo retention in both single mutants and in double mutants without increase in the number of laid embryos on the plate, suggesting defective embryogenesis. In all mutants, we also observed gross disturbances in anatomy. This was most marked in the gut and in the germ line, with defects including

amorphous substance accumulation, vacuoles, indistinguishable internal organ structure, organ malformations, and augmentation of compartments. The enterocytic cytoplasm was more coarsely granulated, particularly in *plin-1* and *hosl-1* mutant animals (Fig. 1F–N).

The remaining lipid content was determined *in situ* by staining surviving animals by the LipidTox Red fluorescent dye and acquiring fluorescent microscopy images. Controls had small regular LipidTox-positive structures in the enterocyte cytoplasm, while *plin-1* and particularly *hosl-1* mutants had larger LipidTox-positive structures. In double mutant enterocytes, these structures were larger than in controls but smaller than in *hosl-1* mutants (Fig. 2A–H). Morphometric analysis performed on four to six animals per line confirmed this increase in the size of LipidTox-positive structures, defined as an area with an above-threshold intensity in a z-position with the most intense signal. As expected, in *hosl-1* mutants, LipidTox-positive structures occupied the largest area, followed by *plin-1* mutants and *plin-1 hosl-1* double mutants, and finally controls with smallest fluorescent area (Fig. 1I).

### *Lack of PLIN-1 leads to increased accumulation of autophagic marker LGG-1 in early embryos*

To assess the rate of autophagy in early embryos, we used the RD204 line expressing GFP-tagged LGG-1, a most commonly used marker of autophagy in *C. elegans* (Meléndez et al., 2003; Zhang et al., 2015; Chen et al., 2017), with stage-specific promoter  $P_{pie-1}$  used to overcome the general embryonic silencing of transcripts (Manil-Ségalen et al., 2014). This line was crossed with the *plin-1(KV1)* null mutant, and both the crossed line called KV2 and the original RD204 control line were imaged by confocal microscopy and CARS (Fig. 3A–H). A minimum of 10 embryos per line were imaged and the images were quantified (Fig. 3I).

Early embryos of one- to four-cell stage had small foci of GFP signal and small LDs in their cytoplasm, as shown by CARS imaging. The loss of PLIN-1 led to an approximate 3-fold increase in the total volume, surface, number, and integrated intensity of GFP-positive structures and an approximate 4-fold increase in volume, surface, number, and integrated scattering intensity of LDs, as shown by CARS in the same embryos. While the LGG-1-positive structures and LDs seemed to increase in the absence of PLIN-1 in a comparable manner, they did not show significant colocalization in either of the two lines.

## Discussion

In mammalian adipocytes, fasting activates PKA, which phosphorylates PLINs. Activated PLINs, most importantly PLIN-1, then stimulate lipases including HSL, to catabolize stored fats (Sztalryd and Brasaemle, 2017). In *C. elegans*, cold exposure leads to similar activation of PKA and eventually HOSL-1, breaking down

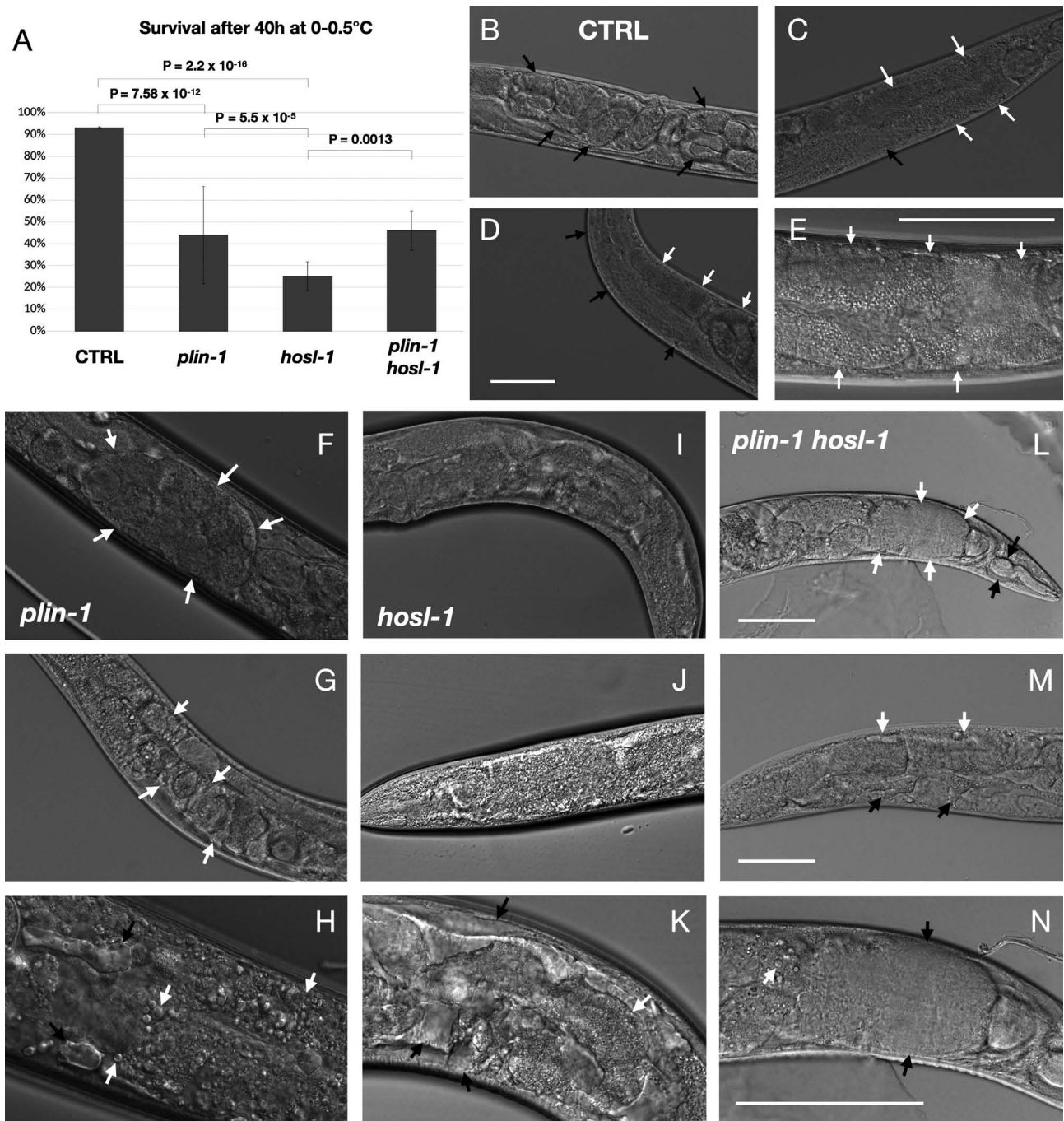


**Fig. 1.** Lipolysis-dependent cold resistance decreases in *plin-1* and *hosl-1* mutants. (A) Survival of *plin-1* and *hosl-1* single and double mutants after a 40-h exposure to temperatures of 0–0.5 °C. In the control line, 93 % of animals survived these conditions, while only 25 % of *hosl-1(tm2369)* mutants and 44 % of *plin-1(KV1)* mutants survived. Interestingly, the loss of PLIN-1 in *hosl-1* mutants resulted in a partial rescue of the phenotype, with a survival rate of 46 %. (B)–(N) Nomarski optics microscopy images of surviving animals in individual lines, taken at two different magnifications. In control animals (B)–(E), cold induces a physiological reaction of embryo retention (black arrows in B), but the internal anatomy is mostly undisturbed. Proximal germ line (black arrows in C and D), oocytes and embryos (white arrows in D), as well as the gut (white arrows in C and E) have normal or only slightly distorted forms. Contrarily, *plin-1(KV1)* (F)–(H), *hosl-1(tm2369)* (I)–(K) and double mutants (L)–(N) have severe malformations such as extracellular accumulation of amorphous substance (arrows in F and G), vacuoles (black arrows in H, K and M), indistinguishable internal organ structure (I)–(K), (M), organ malformations (white arrow in K), and augmentation of compartments (black arrows in N). The enterocyte cytoplasm is also more coarsely granulated (white arrows in H and N). Defects in gonad structure result in decreased embryo retention. Gene names in pictures indicate the names of knocked-out genes in the given lines, CTRL is control. Bars indicate 100 µm.

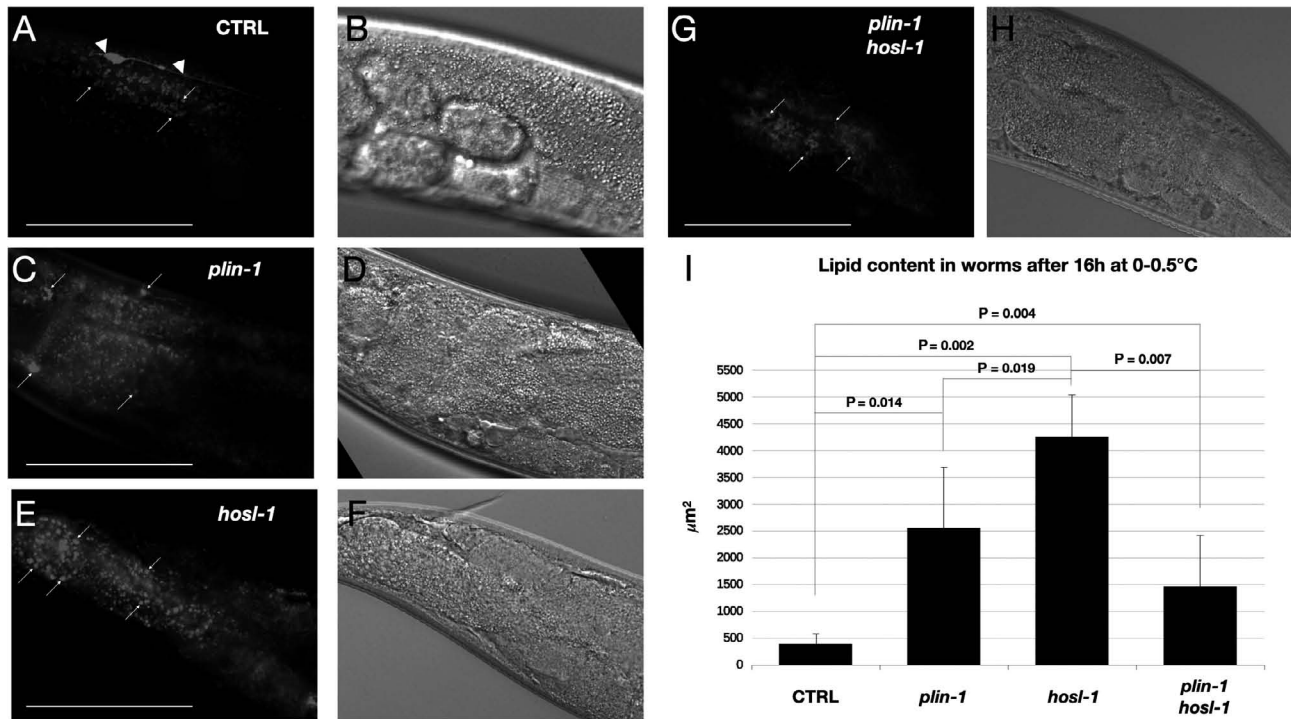


**Fig. 2.** Lipid content analysis in animals surviving cold exposure. (A)-(H) Lipid content visualization in the cold-surviving animals by a red channel fluorescent microscopy of LipidTox-stained fixed animals with corresponding Nomarski optics bright-field images. Equivalent whole-image brightness and contrast adjustment were applied. Lipid droplets (arrows) in the control line are small round structures with little residual lipid content (A). An increase of the lipid content is seen in both *plin-1* (B) and especially *hosl-1* (C) mutants and to a milder degree in the double mutants (D). Arrowheads in (A) show unrelated fluorescence of a neuron cell used as a selection marker in the VS20 control line (excluded from quantification). (E) Morphometric analysis of four to six biological replicates per line stained by LipidTox and imaged by fluorescent microscopy. The surface area of structures was 6.6-times larger in *plin-1*-deficient animals, 11-times larger in *hosl-1*-deficient animals and 3.7-times larger in double mutants when compared to controls. Error bars represent standard deviations. Gene names in pictures indicate the names of knocked-out genes in the given lines, CTRL is control. Bars indicate 100  $\mu\text{m}$  and (A)-(H) are to scale.

TAGs and producing cryoprotective glycerol (Liu et al., 2017). It is therefore likely that were *C. elegans* PLIN-1 homologous to mammalian PLINs, it would also regulate HOSL-1. Our results show that intact PLIN-1 is required for protection of animals against cold (Fig. 1A) and that animals lacking PLIN-1 have augmented LDs with more neutral lipids (Fig. 2C and 2I). This suggests that in the absence of PLIN-1, HOSL-1-dependent lipolysis is impaired. Moreover, in the absence of PLIN-1, the presence or absence of HOSL-1 does not influence survival in cold nor the residual lipid content, *i.e.*, *plin-1* single mutants and *plin-1 hosl-1* double mutants did not significantly differ in these attributes (Figs. 1A, 2C, 2G and 2I). PLIN-1 might therefore be needed for activation of HOSL-1 by PKA, placing it in between PKA and HOSL-1 in the regulatory pathway.

Interestingly, the severe phenotypes of *hosl-1(tm2369)* animals were partially rescued in animals also lacking PLIN-1 (Fig. 1A and 1L-N) and these double mutants had less lipids than the *hosl-1* mutants (Fig. 2G and 2I). Survival and lipid content in these double mutants were

similar to those of *plin-1* single mutants. One possible explanation would be that an alternative glycerol-generating pathway exists, which is suppressed by activated PLIN-1. In the absence of PLIN-1, such pathway would be disinhibited and provide a certain amount of glycerol. The *hosl-1 plin-1* double mutants have less lipids than *hosl-1* single mutants (Fig. 2I), suggesting that this alternative pathway of glycerol production is a lipolytic pathway.

Physiologically, early embryos are known to form small autophagic clusters involved in clearance of paternal organelles, as described previously (Manil-Ségalen et al., 2014; Djeddi et al., 2015). The loss of PLIN-1 results in formation of larger, more numerous perinuclear LGG-1-positive structures (Fig. 3F and 3I-L). At the same time, PLIN-1-deficient embryos form perinuclear clusters of neutral lipids, as visualized by CARS (Fig. 3E). The presence of larger cytoplasmic clusters of LGG-1 suggests increased autophagic activity in the absence of PLIN-1, partially overlapping with the augmented stores of neutral lipids. This provides an indica-

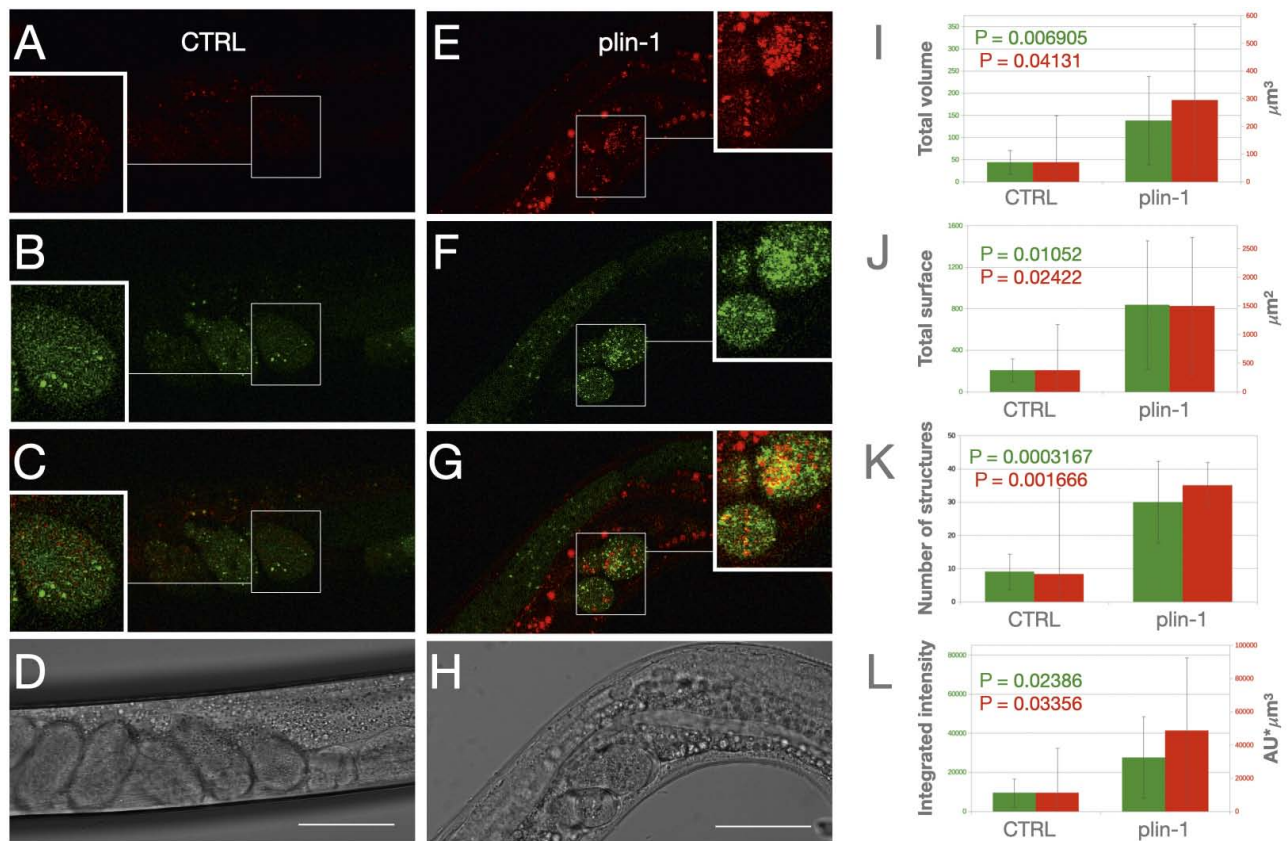


**Fig. 3.** Colocalization of lipids and autophagic marker LGG-1 in early embryogenesis. (A)-(H) Representative images of a RD204 [ $P_{pie-1}::lgg-1::gfp$ ] control line (A)-(D) and of the KV2 [ $P_{pie-1}::lgg-1::gfp; plin-1(KV1)$ ] line (E)-(H). (A) and (E) CARS diagram centred on early embryos. (B) and (F), corresponding GFP images of the same  $xyz$  coordinates showing subcellular localization of LGG-1, a marker of autophagy. (C) and (G), fused-channel images of GFP and CARS. (D) and (H), bright-field microscopy images of the corresponding focal planes. (I)-(L) Morphometric analysis of 15.4  $\mu\text{m}$  z-stacks of CARS diagrams (left column) and GFP images (right column) of earliest embryos for each of RD204 (N = 11) and KV2 (N = 10) lines, respectively. Whole-image contrast and brightness adjustments were applied, same to both experiment and control. GFP images are presented in green and CARS diagrams in red pseudo-colours. Bars indicate 50  $\mu\text{m}$  and images (A)-(H) are to scale. Insets in images (A)-(C) and (E)-(G) are magnified and increased in brightness. P values in images (first line: GFP, second line: CARS).

tion that PLIN-1 inhibits the rate of autophagy in certain conditions and that this autophagy might mediate lipolysis.

Taken together, our results indicate that PLIN-1 regulates HOSL-1 positively, as is the case of mammalian PLINs, and that it might regulate some forms of autophagy, possibly lipophagy, in *C. elegans* negatively.

#### Acknowledgements

Authors thank Dr. Renaud Legouis for providing the RD204 line, Dr. Zdeněk Kostrouch and Dr. Vladimír Saudek for valuable suggestions. Authors thank the Imaging Methods Core Facility of Biocev, supported by the MEYS CR (Large RI Project LM2018129 Czech-BioImaging) and ERDF (project No. CZ.02.1.01/0.0/0.0/16\_013/0001775) for cooperation in confocal and CARS microscopy.

#### References

- Chen Y., Scarcelli, V., Legouis, R. (2017) Approaches for studying autophagy in *Caenorhabditis elegans*. *Cells* **6**, 27.
- Chughtai, A. A., Kaššák, F., Kostrouchová, M., Novotný, J. P., Krause, M. W., Saudek, V., Kostrouch, Z., Kostrouchová, M. (2015) Perilipin-related protein regulates lipid metabolism in *C. elegans*. *PeerJ* **2015**, e1213.
- Cingolani, F., Czaja, M. J. (2016) Regulation and functions of autophagic lipolysis. *Trends Endocrinol. Metab.* **27**, 696-705.
- Djeddi, A., Rawi, S., Deuve, J. L., Perrois, C., Liu, Y.-Y., Russeau, M., Sachse, M., Galy, V. (2015) Sperm-inherited organelle clearance in *C. elegans* relies on LC3-dependent autophagosome targeting to the pericentrosomal area. *Development* **142**, 1705-1716.
- Liu, F., Xiao, Y., Ji, X.-L., Zhang, K.-Q., Zou, C.-G. (2017) The cAMP-PKA pathway-mediated fat mobilization is required for cold tolerance in *C. elegans*. *Sci. Rep.* **7**, 638.

- Manil-Ségalen, M., Lefebvre, C., Jenzer, C., Trichet, M., Boulogne, C., Satiat-Jeuemaitre, B., Legouis, R. (2014) The *C. elegans* LC3 acts downstream of GABARAP to degrade autophagosomes by interacting with the HOPS subunit VPS39. *Dev. Cell* **28**, 43-55.
- Meléndez, A., Tallóczy, Z., Seaman, M., Eskelinen, E.-L., Hall, D. H., Levine, B. (2003) Autophagy genes are essential for dauer development and life-span extension in *C. elegans*. *Science* **301**, 1387-1391.
- Na, H., Zhang, P., Chen, Y., Zhu, X., Liu, Y., Liu, Y., Xie, K., Xu, N., Yang, F., Yu, Y., Cichello, S., Mak, H. Y., Wang, M. C., Zhang, H., Liu P. (2015) Identification of lipid droplet structure-like/resident proteins in *Caenorhabditis elegans*. *Biochim. Biophys. Acta* **1853**, 2481-2491.
- O'Rourke, E. J., Soukas, A. A., Carr, C. E., Ruvkun, G. (2009) *C. elegans* major fats are stored in vesicles distinct from lysosome-related organelles. *Cell Metab.* **10**, 430-435.
- R Core Team (2014) *R: A language and environment for statistical computing*.
- Schindelin, J., Arganda-Carreras, I., Frise, E., Kaynig, V., Longair, M., Pietzsch, T., Preibisch, S., Rueden, C., Saalfeld, S., Schmid, B., Tinevez, J. Y., White, D. J., Hartenstein, V., Eliceiri, K., Tomancak, P., Cardona, A. (2012) Fiji: an open-source platform for biological-image analysis. *Nat. Methods* **9**, 676-682.
- Singh, R., Kaushik, S., Wang, Y., Xiang, Y., Novak, I., Komatsu, M., Tanaka, K., Cuervo, A. M., Czaja, M. J. (2009) Autophagy regulates lipid metabolism. *Nature* **458**, 1131-1135.
- Stiernagle, T. (2006) Maintenance of *C. elegans*. *WormBook* 1-11.
- Subramanian, V., Rothenberg, A., Gomez, C., Cohen, A. W., Garcia, A., Bhattacharyya, S., Shapiro, L., Dolios, G., Wang, R., Lisanti, M. P., Brasaemle, D. L. (2004) Perilipin A mediates the reversible binding of CGI-58 to lipid droplets in 3T3-L1 adipocytes. *J. Biol. Chem.* **279**, 42062-42071.
- Sztralryd, C., Xu, G., Dorward, H., Tansey, J. T., Contreras, J. A., Kimmel, A. R., Londos, C. (2003) Perilipin A is essential for the translocation of hormone-sensitive lipase during lipolytic activation. *J. Cell Biol.* **161**, 1093-1103.
- Sztralryd, C., Brasaemle, D. L. (2017) The perilipin family of lipid droplet proteins: Gatekeepers of intracellular lipolysis. *Biochim. Biophys. Acta Mol. Cell Biol. Lipids* **1862**, 1221-1232.
- Vrablik, T. L., Petyuk, V. A., Larson, E. M., Smith, R. D., Watts, J. L. (2015) Lipidomic and proteomic analysis of *Caenorhabditis elegans* lipid droplets and identification of ACS-4 as a lipid droplet-associated protein. *Biochim. Biophys. Acta* **1851**, 1337-1345.
- Zhang, H., Chang, J. T., Guo, B., Hansen, M., Jia, K., Kovács, A. L., Kumsta, C., Lapierre, L. R., Legouis, R., Lin, L., Lu, Q., Meléndez, A., O'Rourke, E. J., Sato, K., Sato, M., Wang, X., Wu, F. (2015) Guidelines for monitoring autophagy in *Caenorhabditis elegans*. *Autophagy* **11**, 9-27.